Comparison of Early-Phase ^{11}C-Deuterium-L-Deprenyl and ^{11}C-Pittsburgh Compound B PET for Assessing Brain Perfusion in Alzheimer Disease

Elena Rodriguez-Vieitez[1], Stephen F. Carter[1,2], Konstantinos Chiotis[1], Laure Saint-Aubert[1], Antoine Leuzy[1], Michael Schöll[1], Ove Almkvist[1,3,4], Anders Wall[5], Bengt Långström[6], and Agneta Nordberg[1,4]

[1]Division of Translational Alzheimer Neurobiology, Center for Alzheimer Research, Department of Neurobiology, Care Sciences and Society, Karolinska Institutet, Stockholm, Sweden; [2]Wolfson Molecular Imaging Centre, Institute of Brain, Behaviour and Mental Health, University of Manchester, Manchester, United Kingdom; [3]Department of Psychology, Stockholm University, Stockholm, Sweden; [4]Department of Geriatric Medicine, Karolinska University Hospital Huddinge, Stockholm, Sweden; [5]Department of Surgical Sciences, Section of Nuclear Medicine & PET, Uppsala University, Uppsala, Sweden; and [6]Deparment of Chemistry, Uppsala University, Uppsala, Sweden

The PET tracer ^{11}C-deuterium-L-deprenyl (^{11}C-DED) has been used to visualize activated astrocytes in vivo in patients with Alzheimer disease (AD). In this multitracer PET study, early-phase ^{11}C-DED and ^{11}C-Pittsburgh compound B (^{11}C-PiB) (eDED and ePiB, respectively) were compared as surrogate markers of brain perfusion, and the extent to which ^{11}C-DED binding is influenced by brain perfusion was investigated. **Methods:** ^{11}C-DED, ^{11}C-PiB, and ^{18}F-FDG dynamic PET scans were obtained in age-matched groups comprising AD patients (n = 8), patients with mild cognitive impairment (n = 17), and healthy controls (n = 16). A modified reference Patlak model was used to quantify ^{11}C-DED binding. A simplified reference tissue model was applied to both ^{11}C-DED and ^{11}C-PiB to measure brain perfusion relative to the cerebellar gray matter (R_1) and binding potentials. ^{11}C-PiB retention and ^{18}F-FDG uptake were also quantified as target-to-pons SUV ratios in 12 regions of interest (ROIs). **Results:** The strongest within-subject correlations with the corresponding R_1 values ($R_{1,DED}$ and $R_{1,PiB}$, respectively) and with ^{18}F-FDG uptake were obtained when the eDED and ePiB PET data were measured 1–4 min after injection. The optimum eDED/ePiB intervals also showed strong, significant ROI-based intersubject Pearson correlations with $R_{1,DED}/R_{1,PiB}$ and with ^{18}F-FDG uptake, whereas ^{11}C-DED binding was largely independent of brain perfusion, as measured by eDED. Corresponding voxelwise correlations confirmed the ROI-based results. Temporoparietal eDED or ePiB brain perfusion measurements were highly discriminative between patient and control groups, with discriminative ability statistically comparable to that of temporoparietal ^{18}F-FDG glucose metabolism. Hypometabolism extended over wider regions than hypoperfusion in patient groups compared with controls. **Conclusion:** The 1- to 4-min early-frame intervals of ^{11}C-DED or ^{11}C-PiB are suitable surrogate measures for brain perfusion. ^{11}C-DED binding is independent of brain perfusion, and thus ^{11}C-DED PET can provide information on both functional (brain perfusion) and pathologic (astrocytosis) aspects from a single PET scan. In comparison with glucose metabolism, early-phase ^{11}C-DED and ^{11}C-PiB perfusion appear to provide complementary rather than redundant information.

Key Words: amyloid; astrocytosis; brain perfusion; early-phase PET

J Nucl Med 2016; 57:1071–1077
DOI: 10.2967/jnumed.115.168732

The new diagnostic criteria for Alzheimer disease (AD) (*1,2*) include the use of molecular imaging biomarkers. Recently, the PET amyloid-β (Aβ) tracers ^{18}F-florbetapir, ^{18}F-flutemetamol, and ^{18}F-florbetaben were approved by the European Medicines Agency and by the U.S. Food and Drug Administration for assessing the presence of Aβ pathology in individuals with early memory disorders. Biomarkers are classified as either pathophysiologic, indicating the presence of Aβ or tau pathology, or topographic, reflecting disease progression (*2*). The expanding clinical application of PET imaging biomarkers has motivated research on dual-use application of ^{11}C-Pittsburgh compound B (^{11}C-PiB) and ^{18}F-florbetapir to measure both pathologic (Aβ) and functional (brain perfusion) parameters (*3,4*), potentially reducing costs and patient burden, especially if the brain perfusion measurement provides information that is closely related to that from an ^{18}F-FDG PET scan.

The first study on the dual use of ^{11}C-PiB PET (*5*) found that the K_1 influx constant from arterial blood sampling and the 0- to 6-min early time-averaged frames were both suitable measures of brain perfusion in healthy and AD brains. Subsequent studies using early-phase intervals of 0–6 min or 1–8 min found that these were reliable times to measure brain perfusion. The results were closely correlated with ^{18}F-FDG PET glucose metabolism results (*3,6–8*), consistent with previous observations that brain perfusion and glucose metabolism are generally related (*9*). The 1- to 6-min early-phase ^{18}F-florbetapir results have also successfully measured perfusion (*4*).

Although the accumulation of Aβ plaques in the brain is thought to play a causative role in AD (*10*), there is increasing evidence that glial activation and neuroinflammation (*11*) could contribute to disease development, and thus there is a growing interest in PET imaging of activated glial cells (*12*). The PET tracer ^{11}C-deuterium-L-deprenyl (^{11}C-DED) binds to monoamine oxidase-B, which is overexpressed in reactive astrocytes (*13*), and has been used to investigate astrocytosis in neurodegenerative diseases including

Received Oct. 27, 2015; revision accepted Jan. 29, 2016.
For correspondence or reprints contact: Agneta Nordberg, Karolinska Institutet, Department of Neurobiology, Care Sciences and Society, Division of Translational Alzheimer Neurobiology, Novum 5th Floor, Blickagången 6, Huddinge, SE-141 57 Stockholm, Sweden.
E-mail: Agneta.K.Nordberg@ki.se
Published online Feb. 16, 2016.

AD (*14,15*). ^{11}C-DED binding is significantly higher in prodromal AD patients than in dementia patients or healthy controls (HCs) (*15*), and ^{11}C-DED binding in prodromal AD patients is negatively correlated with gray matter (GM) density (*16*).

Deuterium was incorporated into ^{11}C-DED to reduce the influence of brain perfusion on tracer binding (*17*). Previous studies (*17,18*) reported high first-pass extraction from blood (K_1 influx constant). However, no study has yet investigated the suitability of early-phase ^{11}C-DED as a surrogate marker for brain perfusion or the relationship of this surrogate to ^{11}C-DED binding; the latter could help to assess whether ^{11}C-DED binding (*15,16*) might be significantly affected by brain perfusion differences among diagnostic groups.

We hypothesized that early-phase ^{11}C-DED and ^{11}C-PiB PET would be suitable surrogate markers of brain perfusion. To this end, we used a multitracer (^{11}C-DED, ^{11}C-PiB, and ^{18}F-FDG) PET imaging approach with the following aims: to investigate the optimum early-phase intervals of ^{11}C-DED and ^{11}C-PiB PET uptake that represent reliable markers of brain perfusion; to establish the independence of ^{11}C-DED from brain perfusion, to demonstrate the potential dual-use of ^{11}C-DED to simultaneously measure brain perfusion and astrocytosis in a single PET scan; and to compare the diagnostic potential of brain perfusion (measured by early-phase ^{11}C-DED and ^{11}C-PiB) with that of glucose metabolism (measured by ^{18}F-FDG), by evaluating their ability to discriminate between patient and control groups.

MATERIALS AND METHODS

Study Participants

This study involved 41 participants including 17 mild cognitive impairment (MCI) patients, 8 AD patients, and 16 HCs, all recruited at the Department of Geriatric Medicine, Karolinska University Hospital Huddinge (Sweden) for another multitracer PET study (*15*). All controls, patients, and caregivers provided written informed consent to participate in the study, which was conducted according to the Declaration of Helsinki and subsequent revisions. Ethical approval was obtained from the Regional Human Ethics Committee of Stockholm and the Faculty of Medicine and Radiation Hazard Ethics Committee of Uppsala University Hospital, Uppsala, Sweden. Participants underwent a comprehensive clinical and imaging examination including medical history, physical examination, MRI, blood sample *APOE* genotyping, neuropsychologic assessment, and (patients only) cerebrospinal fluid analysis (*15*).

The diagnosis of MCI was based on Petersen's criteria (*19*), and AD dementia was diagnosed according to National Institute of Neurologic and Communicative Disorders and Stroke, and the Alzheimer Disease and Related Disorders Association criteria (*20*). A geriatrician/neurologist, a neuropsychologist, and a nurse made diagnoses during a consensus meeting. MCI patients were classified as ^{11}C-PiB–positive (PiB+) or ^{11}C-PiB–negative (PiB–) using a cutoff neocortical SUVR of 1.41 with reference to the cerebellar GM, as previously described (*21*). The PiB+ MCI patients fulfilled the current diagnostic criteria for prodromal AD (*2*). Participant demographic and clinical data are shown in Table 1; all groups were matched for age and sex.

Imaging Methodology

Image Acquisition and Processing. Participants underwent ^{11}C-DED, ^{11}C-PiB, and ^{18}F-FDG PET examinations at the Uppsala PET Center on ECAT EXACT HR+ (Siemens/CTI) and Discovery ST PET/CT (GE Healthcare) scanners. The tracers were produced, and the PET and MR image acquisition and processing methods were set as previously described (*15*). Briefly, the T1 MR image for each participant was coregistered onto the individual's 10- to 60-min late-sum ^{11}C-DED image using SPM8 (Wellcome Trust Centre for Neuroimaging at UCL); 40- to 60-min ^{11}C-PiB and 30- to 45-min ^{18}F-FDG late-sum images were coregistered onto the T1 MR image (which had been previously coregistered to ^{11}C-DED space). A simplified probabilistic atlas (*22*) consisting of 12 bilateral regions of interest (ROIs) was registered from the

TABLE 1
Participant Information

Characteristic	HC (n = 16)	MCI (n = 17)		AD (n = 8)
		PiB− MCI (n = 4)	PiB+ MCI (n = 13)	
Sex	10 M/6 F	2 M/2 F	7 M/6 F	5 M/3 F
Age (y)	51.1 (14.2)	61.8 (7.5)	62.0 (6.4)	63.0 (6.5)
Education (y)	11.1 (2.0)	13.8 (2.2)	13.7 (2.3)	11.0 (2.3)
APOE4+ carriers (%)	5 (31%)	1 (25%)	10 (77%)*	6 (75%)*
Mini-Mental State Examination score	28.9 (1.2)	27.3 (2.1)	27.8 (1.8)	23.8 (5.7)†
Global cognition (z score)	0.13 (0.66)	−0.31 (0.80)	−0.70 (0.95)	−2.07 (2.03)‡
Episodic memory (z score)	−0.11 (0.48)	−1.20 (0.91)	−1.36 (0.72)	−2.25 (0.72)‡
Cerebrospinal fluid data (pg/mL)¶				
Aβ42		1160 (203)	537 (148)	506 (158)
Total τ		257 (46)	404 (152)	608 (321)
Phospho τ		55 (20)	67 (16)	93 (30)

*Significantly higher than HC (χ^2 test).
†Significantly lower than HC (Mann–Whitney test).
‡Global cognition and episodic memory z scores < -1.645 are considered outside cognitively normal reference range; neuropsychologic test description was previously reported (*15*).
¶Cerebrospinal fluid data are considered abnormal for Aβ42 $<$ 550 pg/mL, total τ $>$ 400 pg/mL, and phospho τ $>$ 60 pg/mL.
Values are means (SDs) or number (%).

Montreal Neurologic Institute space onto the subject's ^{11}C-DED space and was masked using individual GM masks. Registered ^{18}F-FDG and ^{11}C-PiB PET images were sampled using these individual cortical atlases; the whole pons was used as a reference.

PET Kinetic Modeling

^{11}C-PiB PET. Regional time–activity curves were extracted from dynamic ^{11}C-PiB PET data using PMOD (version 3.3; PMOD Technologies Ltd.). The time–activity curves were fitted to the simplified reference tissue model (*23*) implemented in PMOD with the cerebellar GM as a reference, and kinetic parameters were obtained for brain perfusion relative to cerebellar GM ($R_{1,PiB}$) and for nondisplaceable binding potential ($BP_{ND,PiB}$).

^{11}C-DED PET. The regional ^{11}C-DED time–activity curves were fitted using 2 reference tissue models. A modified reference Patlak model, previously validated against a model using arterial sampling (*17*), was applied to the ^{11}C-DED time–activity curves using the cerebellar GM as a reference, as previously described (*15*); ^{11}C-DED binding was thus estimated by the Patlak slope (min^{-1}). The simplified reference tissue model implemented in PMOD was also applied to the ^{11}C-DED time–activity curves using the cerebellar GM as a reference, and the corresponding regional kinetic parameters for brain perfusion relative to cerebellar GM ($R_{1,DED}$) and for nondisplaceable binding potential ($BP_{ND,DED}$) were thus obtained.

Optimization of Early-Frame Time Intervals for ^{11}C-DED and ^{11}C-PiB

A range of time-averaged early-frame ^{11}C-DED (eDED) and ^{11}C-PiB (ePiB) PET intervals were generated in PMOD, using several initial time points (t_0 = 0, 0.5, 1, and 2 min) and interval durations (0.5–10 min). Specifically, regional time–activity curves were integrated over each early-frame interval and subsequently normalized to the integrated time–activity curve of the cerebellar GM reference during the same period. Six randomly selected participants (2 AD, 2 MCI, and 2 HC participants) were used for within-subject correlations for eDED versus $R_{1,DED}$, ePiB versus $R_{1,PiB}$, and eDED/ePiB versus ^{18}F-FDG, across 24 regions extracted from the Hammers atlas (*22*). For all early-frame intervals investigated, the individual within-subject Pearson correlation coefficients were subsequently averaged across the 6 participants. The early-frame interval corresponding to the maximum Pearson r (mean ± SD) was deemed optimum and selected for the remainder of the study.

Evaluation of Early-Phase ^{11}C-DED and ^{11}C-PiB PET as Surrogate Measures of Brain Perfusion

To evaluate eDED and ePiB as markers of brain perfusion, regional intersubject Pearson correlations were performed for eDED versus $R_{1,DED}$, eDED versus ^{18}F-FDG, ePiB versus $R_{1,PiB}$, and ePiB versus ^{18}F-FDG. A representative neocortical (frontal, parietal, and temporal) composite ROI was also used to perform correlation and linear regression analyses between the same pairs of variables. To assess the influence of brain perfusion on ^{11}C-DED binding and ^{11}C-PiB retention, regional intersubject correlations were performed for eDED versus the ^{11}C-DED Patlak slope and for ePiB versus the ^{11}C-PiB SUVR. In addition, voxelwise correlations were performed to verify the above-mentioned ROI-based analyses.

Statistics

ROI-Based Analyses. All correlation analyses were performed using a 2-tailed Pearson product-moment coefficient. The significance level was a P value of less than 0.05. To account for multiple comparisons across 12 ROIs, a Bonferroni-corrected threshold of P less than 0.004 was set as appropriate. Receiver-operating-characteristic analysis was used to compare the discriminative abilities of eDED, ePiB, and ^{18}F-FDG by obtaining the areas under the curve (AUCs) for classifying patient groups versus the HCs; the DeLong test was used to evaluate whether the eDED, ePiB, and ^{18}F-FDG AUCs were significantly different. Statistical analyses were performed using SPSS (version 22.0; IBM Corp.) and the pROC package in R (version 3.1.2; R Foundation for Statistical Computing).

Voxelwise Analyses. Voxelwise analyses were performed using biologic parametric mapping (version 3.3) (*24*) for multimodal image correlations and the statistical parametric mapping (SPM8) 2-sample t test for group comparisons. PET images were first registered onto the Montreal Neurologic Institute space, then smoothed by a gaussian filter of 8 mm in full width at half maximum and masked by a GM mask. Biologic parametric mapping correlation maps and SPM8 T-maps were thresholded at a P value of 0.001 (uncorrected, ≥ 20-voxel cluster extent) and projected onto a template cortical surface using FreeSurfer (version 5.3; surfer.nmr.harvard.edu); clusters that remained significant after familywise error ($P < 0.05$) correction for multiple comparisons were tabulated.

RESULTS

Evaluation of ^{11}C-DED and ^{11}C-PiB Quantification Approaches

The regional ^{11}C-DED Patlak slopes were highly consistent with their respective $BP_{ND,DED}$ values (intersubject neocortical Pearson $r = 0.90$; $P < 0.001$) (Supplemental Fig. 1A; supplemental materials are available at http://jnm.snmjournals.org). Similarly, regional $BP_{ND,PiB}$ and ^{11}C-PiB SUVRs were significantly correlated (intersubject neocortical Pearson $r = 0.91$; $P < 0.001$) (Supplemental Fig. 1B). Detailed regional correlations are included in Supplemental Table 1.

Selection of Optimum eDED and ePiB Intervals

Figure 1 depicts, for each start time and interval duration investigated, the within-subject (mean ± SD) Pearson r correlation coefficients between eDED and $R_{1,DED}$/^{18}F-FDG and between ePiB and $R_{1,PiB}$/^{18}F-FDG. Intervals including the first minute of the scan resulted in low correlation coefficients, probably due to an initially noisy signal. When eDED (Fig. 1A) and ePiB (Fig. 1B) records started at t_0 = 1 min, maximum correlation coefficients were observed for a 3-min interval. Both eDED and ePiB showed stronger associations with their respective R_1 values (with maximum $r \sim 0.98$) than with ^{18}F-FDG (peaking at $r \sim 0.80$). The 1- to 4-min frame was thus selected as optimum for the remainder of the study. eDED and ePiB showed somewhat different patterns of within-subject association with ^{18}F-FDG (Fig. 1): although the association between eDED and ^{18}F-FDG started to decline beyond the optimum 1- to 4-min eDED frame, ePiB and ^{18}F-FDG remained highly associated for intervals up to 10 min in duration.

Depictions of representative 1- to 4-min eDED and ePiB PET scans and ^{11}C-DED, ^{11}C-PiB, and ^{18}F-FDG uptake (Fig. 2) show that the eDED and ePiB scans were visually similar to those for ^{18}F-FDG but different from those for ^{11}C-DED and ^{11}C-PiB.

Early-Phase ^{11}C-DED and ^{11}C-PiB as PET Markers of Brain Perfusion

The regional intersubject correlations (Table 2) between eDED and $R_{1,DED}$ and between ePiB and $R_{1,PiB}$ were strong and significant, with neocortical Pearson $r = 0.99$ and 0.96, respectively ($P < 0.001$). The corresponding linear regression slopes nearly reached unity (Fig. 3).

The regional intersubject correlations between eDED and ^{18}F-FDG (Table 2) were also strong and significant except in the putamen, with neocortical Pearson $r = 0.66$ ($P < 0.001$) and the slope of the neocortical linear regression nearly reaching unity (Fig. 3). The neocortical intersubject correlation between ePiB and ^{18}F-FDG

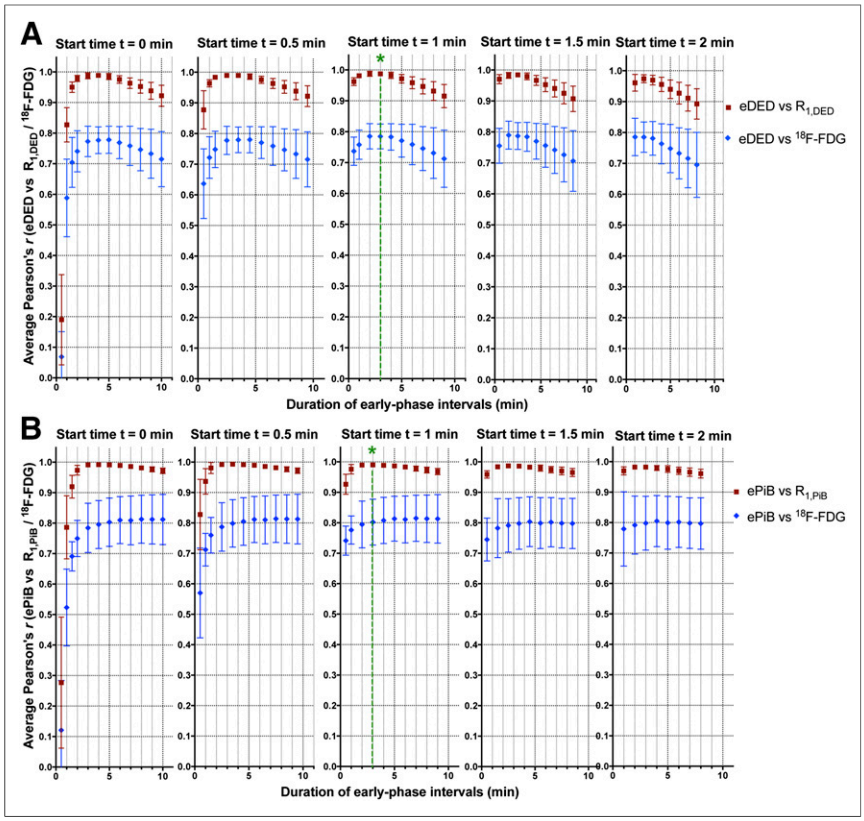

FIGURE 1. Optimization of early-phase intervals for ^{11}C-DED (A) and ^{11}C-PiB (B). Each point represents average ± SD within-subject Pearson correlation coefficient (*r*) for eDED/ePiB vs. respective $R_{1,DED}/R_{1,PiB}$ (red squares) and vs. ^{18}F-FDG (blue diamonds). Optimum 1- to 4-min eDED/ePiB intervals are marked by asterisks.

was strong and significant (Pearson $r = 0.61$; $P < 0.001$), with a linear regression slope close to unity; however, the ePiB versus ^{18}F-FDG regional subcortical correlations were nonsignificant except in the hippocampus (Table 2).

In contrast, eDED and ePiB showed no consistent associations with the ^{11}C-DED Patlak slope or the ^{11}C-PiB SUVR, respectively. For most cortical regions, eDED was not significantly correlated to the ^{11}C-DED Patlak slope, whereas few significant associations were observed in limbic and subcortical regions. None of the ROIs showed a significant correlation between ePiB and the ^{11}C-PiB SUVR (Table 2; Supplemental Fig. 2).

The voxelwise correlation map of eDED and ^{18}F-FDG showed a high degree of overlap across wide cortical areas (Fig. 4A), which remained significant after multiple-comparisons correction in numerous regions including the lateral temporoparietal, frontal, anterior, and posterior cingulate cortices (Supplemental Table 2). In contrast, a low degree of overlap was observed between eDED and ^{11}C-DED Patlak slope parametric images (Fig. 4B), and few clusters (in the inferior frontal gyrus, caudate, and thalamus) remained significant after multiple-comparisons correction (Supplemental Table 2). No significant overlap was observed in any region of ^{18}F-FDG versus the ^{11}C-DED Patlak slope voxelwise correlation map (not shown).

Comparisons Between Brain Perfusion (eDED, ePiB) and Metabolism (^{18}F-FDG) Measures Across Diagnostic Groups

Voxelwise SPM8 group comparisons were performed to investigate the spatial distributions of hypoperfusion (eDED) and hypometabolism in patient groups compared with HCs. In the PiB+ MCI group, hypoperfusion was most significantly observed in left temporoparietal cortical areas, whereas hypometabolism was extended over wider bilateral temporoparietal, posterior cingulate, and frontal regions (Fig. 5; Supplemental Table 3). In AD patients, hypoperfusion was observed in bilateral temporoparietal cortical regions, whereas hypometabolism was more widespread in the bilateral temporoparietal, posterior cingulate, frontal, and occipital cortices (Fig. 5; Supplemental Table 4). Overall, the temporoparietal cortex consistently showed hypoperfusion and hypometabolism in both patient groups, and thus the parietal and temporal cortices were selected to evaluate the discriminative ability of ^{18}F-FDG, eDED, and ePiB between the patient and HC groups (Supplemental Table 5). The 3 PET parameters discriminated between the AD and HC groups well: AUC = 0.97 (^{18}F-FDG), 0.93 (eDED), and 0.84–0.90 (ePiB). Differences among the 3 AUC values were not statistically significant (Supplemental Table 5). Good discrimination was also observed between PiB+ MCI patients and HCs: AUC = 0.90–96 (^{18}F-FDG), 0.78–87 (eDED), and 0.77 (ePiB) (no significant differences).

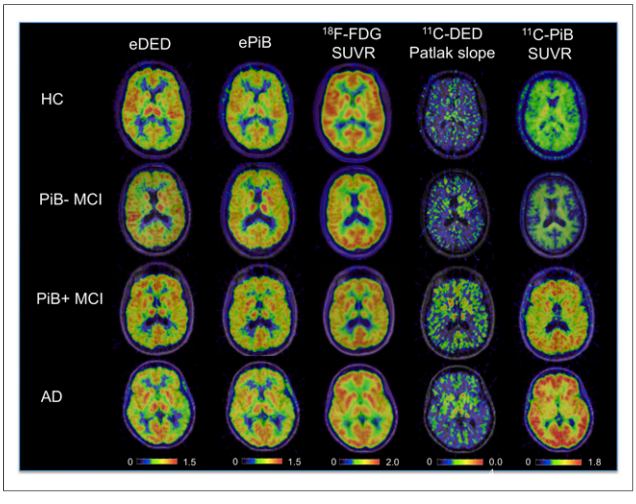

FIGURE 2. Representative PET scans.

DISCUSSION

The results of this study strongly suggest that the early 1- to 4-min PET time frames for the tracers ^{11}C-DED and ^{11}C-PiB can be used to assess brain perfusion. We demonstrated that ^{11}C-DED binding is not strongly influenced by brain perfusion as measured by eDED. Therefore, ^{11}C-DED has dual properties for which the early frames and the tracer binding (as measured by the Patlak slope) measure independent, complementary processes reflecting

TABLE 2
Regional Intersubject Correlations for eDED and ePiB

Region	Intersubject (n = 40) Pearson r correlations					
	eDED			ePiB		
	eDED vs. $R_{1,DED}$	eDED vs. ^{18}F-FDG SUVR	eDED vs. ^{11}C-DED Patlak slope	ePiB vs. $R_{1,PiB}$	ePiB vs. ^{18}F-FDG SUVR	ePiB vs. ^{11}C-PiB SUVR
Cortical						
Frontal	0.992***	0.663***	NS	0.951***	0.512**	NS
Parietal	0.996***	0.677***	NS	0.967***	0.639***	NS
Temporal	0.996***	0.676***	NS	0.973***	0.588***	NS
Occipital	0.983***	0.468**	NS	0.957***	0.446**	NS
Anterior cingulate	0.993***	0.674***	0.554***	0.981***	0.570***	NS
Posterior cingulate	0.975***	0.737***	0.493**	0.945***	NS	NS
Insula	0.996***	0.717***	0.486**	0.985***	0.466**	NS
Parahippocampus	0.984***	0.732***	NS	0.898***	NS	NS
Subcortical						
Caudate	0.977***	0.559***	0.692***	0.977***	NS	NS
Putamen	0.989***	NS	0.465**	0.982***	NS	NS
Thalamus	0.992***	0.635***	0.536***	0.983***	NS	NS
Hippocampus	0.989***	0.649***	NS	0.838***	0.466**	NS

**$P < 0.004$.
***$P < 0.001$.
NS = nonsignificant after Bonferroni adjustment ($P \geq 0.004$).

brain perfusion and astrocytosis, respectively, in a single scan. The dual use of ^{11}C-DED may increase the practical applicability of this tracer, especially because fluorinated compounds are currently under development (*25*). We also confirmed previously reported findings that ^{11}C-PiB binding is not strongly affected by brain perfusion (*26*), providing further support for the dual use of ^{11}C-PiB for perfusion and Aβ measurements.

In our study, the multitracer PET paradigm in the same patients showed that both eDED and ePiB represent surrogate measures of brain perfusion, based on their nearly perfect within- and intersubject correlations with $R_{1,DED}$ and $R_{1,PiB}$, respectively. In addition, we showed that eDED and ePiB were strongly correlated with glucose metabolism (^{18}F-FDG); however, this was at a somewhat lower strength than versus R_1 values.

Both hypoperfusion and hypometabolism were observed in the PiB+ MCI and AD groups, most significantly in the parietotemporal cortex, consistent with the literature (*27,28*) and with the choice of parietotemporal ^{18}F-FDG as biomarker in recent criteria (*1,2*). In the parietotemporal cortex, eDED or ePiB brain perfusion measurements were closely related to ^{18}F-FDG measurements, with similarly high discriminative abilities between patient and control groups. Previous studies have compared in vivo brain perfusion and glucose metabolism measures at different stages of AD and other dementia types. Consistent with our findings, the early frames of Aβ PET tracers including ^{11}C-PiB and ^{18}F-florbetapir showed an ability to discriminate between MCI or AD groups and HCs (*3,4*) and between patients with AD and frontotemporal dementia (*6*) that was similar to that of ^{18}F-FDG. A good correspondence was also found between ^{18}F-FDG PET and perfusion SPECT results in temporoparietal and posterior cingulate cortical regions of AD versus HCs (*27,28*). Perfusion SPECT was somewhat less discriminative than ^{18}F-FDG PET (*29*), probably partly because of its lower spatial resolution.

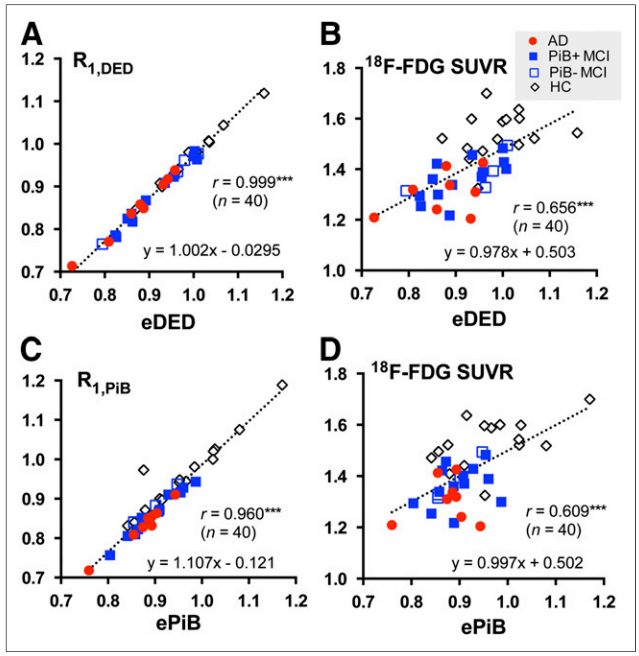

FIGURE 3. Intersubject correlations involving eDED (A and B) and ePiB (C and D) in a neocortical (frontal, temporal, parietal) composite region. ***$P < 0.001$.

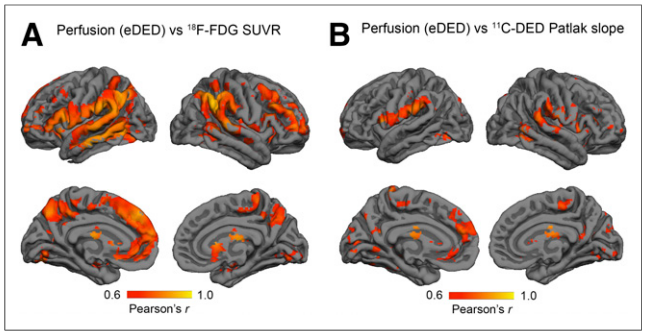

FIGURE 4. Voxelwise correlation maps of eDED vs. ^{18}F-FDG SUVR (A) and eDED vs. ^{11}C-DED Patlak slope (B) using biologic parametric mapping, thresholded at $P < 0.001$ (uncorrected; ≥ 20 voxels).

In our study, we also analyzed the regional distributions of hypoperfusion (as measured by eDED) and hypometabolism in PiB+ MCI and AD patients. Hypometabolism extended over wider brain regions than hypoperfusion, suggesting that perfusion and metabolism are markers of distinct pathophysiologic processes. The finding that hypoperfusion in PiB+ MCI patients predominated in the left hemisphere while hypometabolism was more widespread could indicate that early focal hypoperfusion contributes to hypometabolism in distant but functionally connected regions (*30*). Alternatively, the observation of relatively preserved perfusion in metabolically deficient regions could be explained by vascular regulatory mechanisms to compensate for altered brain metabolism, especially in the early disease stages as previously suggested (*30–32*). Thus, brain perfusion and glucose metabolism could be partially independent but contributory to disease development, consistent with increasing evidence from research on biomarkers including atrophy and hypometabolism, which, despite being closely related, are considered complementary rather than overlapping (*33*).

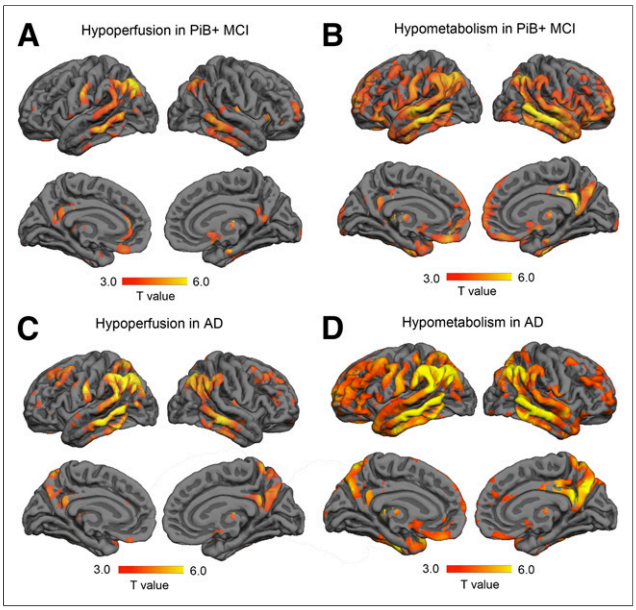

FIGURE 5. Hypoperfusion (early-phase ^{11}C-DED; A and C) and hypometabolism (^{18}F-FDG; B and D) in patient vs. control groups from SPM8 T-maps, thresholded at $P < 0.001$ (uncorrected; ≥ 20 voxels).

Our knowledge is still incomplete regarding the spatiotemporal relationships between different AD biomarkers, including brain perfusion and metabolism, which might not necessarily follow a consecutive progression (*33*). Brain perfusion measurements might contribute to understanding early pathophysiologic changes such as those underlying MCI in the absence of Aβ plaque deposition (suspected nonamyloid pathology) and could be useful as a marker of disease progression or treatment efficacy in clinical trials.

A limitation of our study is the lack of comparison with absolute measures of brain perfusion such those obtained from ^{15}O-H_2O PET or arterial spin labeling MRI or estimated by the washout allometric reference method as demonstrated for ^{11}C-PiB PET (*34,35*). However, multiple measures of brain perfusion relative to the cerebellar GM (eDED, $R_{1,DED}$, ePiB, and $R_{1,PiB}$) and glucose metabolism (^{18}F-FDG) are available for each participant. The study of the discriminative ability of eDED, ePiB, and ^{18}F-FDG was performed with a relatively limited sample size, and further studies will help to confirm the findings.

CONCLUSION

Our findings suggest that the ^{11}C-DED and ^{11}C-PiB PET tracers may have dual functional/pathophysiologic applications, because they allow additional brain perfusion information, distinct from late-phase uptake, to be obtained from a single PET scan. Although brain perfusion and glucose metabolism were shown to be closely related measures, there were also differences between the spatial extents of hypoperfusion and hypometabolism in both PiB+ MCI and AD patient groups, suggesting distinct underlying pathophysiologic mechanisms. The evaluation of brain perfusion from early-phase ^{11}C-DED or ^{11}C-PiB PET scans provides unique, complementary information and therefore adds value, with practical advantages as PET tracers are increasingly used in the clinic.

DISCLOSURE

The costs of publication of this article were defrayed in part by the payment of page charges. Therefore, and solely to indicate this fact, this article is hereby marked "advertisement" in accordance with 18 USC section 1734. This work was financially supported by grants from the Swedish Research Council (project 05817), the Swedish Foundation for Strategic Research, the Knut and Alice Wallenberg Foundation, GE Healthcare (unrestricted grant), the Karolinska Institutet Strategic Neuroscience program, the Stockholm County Council-Karolinska Institutet regional agreement on medical training and clinical research (ALF grant), Swedish Brain Power, the Swedish Brain Foundation, the Alzheimer Foundation in Sweden, the Dementia Association, the EU FP7 large-scale integrating project INMiND (http://www.uni-muenster.de/INMiND), the Foundation for Old Servants, Karolinska Institutet's Foundation for Aging Research, Gun and Bertil Stohne's Foundation, Loo and Hans Osterman's Foundation, the Åhlén Foundation, and the Wenner-Gren Foundation. No other potential conflict of interest relevant to this article was reported.

ACKNOWLEDGMENTS

We are grateful to all participants in the PET studies and their relatives, as well as the staff at the Uppsala PET Center and the Memory Clinic at Karolinska University Hospital, Huddinge. We acknowledge Dr. Rita Almeida for advice on statistical analyses

and thank Johan Lilja for support related to imaging software (VOIager).

REFERENCES

1. McKhann GM, Knopman DS, Chertkow H, et al. The diagnosis of dementia due to Alzheimer's disease: recommendations from the National Institute on Aging-Alzheimer's Association workgroups on diagnostic guidelines for Alzheimer's disease. *Alzheimers Dement.* 2011;7:263–269.
2. Dubois B, Feldman HH, Jacova C, et al. Advancing research diagnostic criteria for Alzheimer's disease: the IWG-2 criteria. *Lancet Neurol.* 2014;13:614–629.
3. Forsberg A, Engler H, Blomquist G, Langstrom B, Nordberg A. The use of PIB-PET as a dual pathological and functional biomarker in AD. *Biochim Biophys Acta.* 2012;1822:380–385.
4. Hsiao IT, Huang CC, Hsieh CJ, et al. Correlation of early-phase ^{18}F-florbetapir (AV-45/Amyvid) PET images to FDG images: preliminary studies. *Eur J Nucl Med Mol Imaging.* 2012;39:613–620.
5. Blomquist G, Engler H, Nordberg A, et al. Unidirectional influx and net accumulation of PIB. *Open Neuroimag J.* 2008;2:114–125.
6. Rostomian AH, Madison C, Rabinovici GD, Jagust WJ. Early ^{11}C-PIB frames and ^{18}F-FDG PET measures are comparable: a study validated in a cohort of AD and FTLD patients. *J Nucl Med.* 2011;52:173–179.
7. Meyer PT, Hellwig S, Amtage F, et al. Dual-biomarker imaging of regional cerebral amyloid load and neuronal activity in dementia with PET and ^{11}C-labeled Pittsburgh compound B. *J Nucl Med.* 2011;52:393–400.
8. Fu L, Liu L, Zhang J, Xu B, Fan Y, Tian J. Comparison of dual-biomarker PIB-PET and dual-tracer PET in AD diagnosis. *Eur Radiol.* 2014;24:2800–2809.
9. Raichle ME. The restless brain: how intrinsic activity organizes brain function. *Philos Trans R Soc Lond B Biol Sci.* 2015;370:20140172.
10. Hardy JA, Higgins GA. Alzheimer's disease: the amyloid cascade hypothesis. *Science.* 1992;256:184–185.
11. Heneka MT, Carson MJ, El Khoury J, et al. Neuroinflammation in Alzheimer's disease. *Lancet Neurol.* 2015;14:388–405.
12. Jacobs AH, Tavitian B, INMiND Consortium. Noninvasive molecular imaging of neuroinflammation. *J Cereb Blood Flow Metab.* 2012;32:1393–1415.
13. Ekblom J, Jossan SS, Bergström M, Oreland L, Walum E, Aquilonius SM. Monoamine oxidase-B in astrocytes. *Glia.* 1993;8:122–132.
14. Santillo AF, Gambini JP, Lannfelt L, et al. In vivo imaging of astrocytosis in Alzheimer's disease: an C-11-L-deuteriodeprenyl and PIB PET study. *Eur J Nucl Med Mol Imaging.* 2011;38:2202–2208.
15. Carter SF, Schöll M, Almkvist O, et al. Evidence for astrocytosis in prodromal Alzheimer disease provided by ^{11}C-deuterium-L-deprenyl: a multitracer PET paradigm combining ^{11}C-Pittsburgh compound B and ^{18}F-FDG. *J Nucl Med.* 2012;53:37–46.
16. Choo IL, Carter SF, Scholl ML, Nordberg A. Astrocytosis measured by ^{11}C-deprenyl PET correlates with decrease in gray matter density in the parahippocampus of prodromal Alzheimer's patients. *Eur J Nucl Med Mol Imaging.* 2014;41:2120–2126.
17. Fowler JS, Wang GJ, Logan J, et al. Selective reduction of radiotracer trapping by deuterium substitution: comparison of carbon-11-L-deprenyl and carbon-11-deprenyl-D2 for MAO B mapping. *J Nucl Med.* 1995;36:1255–1262.
18. Bergström M, Kumlien E, Lilja A, Tyrefors N, Westerberg G, Långström B. Temporal lobe epilepsy visualized with PET with ^{11}C-L-deuterium-deprenyl–analysis of kinetic data. *Acta Neurol Scand.* 1998;98:224–231.
19. Petersen RC. Mild cognitive impairment as a diagnostic entity. *J Intern Med.* 2004;256:183–194.
20. McKhann G, Drachman D, Folstein M, Katzman R, Price D, Stadlan EM. Clinical diagnosis of Alzheimer's disease: report of the NINCDS-ADRDA work group under the auspices of Department of Health and Human Services task force on Alzheimer's disease. *Neurology.* 1984;34:939–944.
21. Nordberg A, Carter SF, Rinne J, et al. A European multicentre PET study of fibrillar amyloid in Alzheimer's disease. *Eur J Nucl Med Mol Imaging.* 2013;40:104–114.
22. Hammers A, Allom R, Koepp MJ, et al. Three-dimensional maximum probability atlas of the human brain, with particular reference to the temporal lobe. *Hum Brain Mapp.* 2003;19:224–247.
23. Lammertsma AA, Hume SP. Simplified reference tissue model for PET receptor studies. *Neuroimage.* 1996;4:153–158.
24. Casanova R, Srikanth R, Baer A, et al. Biological parametric mapping: a statistical toolbox for multimodality brain image analysis. *Neuroimage.* 2007;34:137–143.
25. Nag S, Varrone A, Tóth M, et al. In vivo evaluation in cynomolgus monkey brain and metabolism of [^{18}F]fluorodeprenyl: a new MAO-B pet radioligand. *Synapse.* 2012;66:323–330.
26. Chen YJ, Rosario BL, Mowrey W, et al. PiB relative delivery (R1) as a proxy of relative cerebral blood flow: quantitative evaluation using single session ^{15}O-water and ^{11}C-PiB PET. *J Nucl Med.* 2015;56:1199–1205.
27. Herholz K, Schopphoff H, Schmidt M, et al. Direct comparison of spatially normalized PET and SPECT scans in Alzheimer's disease. *J Nucl Med.* 2002;43:21–26.
28. Matsuda H. Role of neuroimaging in Alzheimer's disease, with emphasis on brain perfusion SPECT. *J Nucl Med.* 2007;48:1289–1300.
29. Silverman DH. Brain ^{18}F-FDG PET in the diagnosis of neurodegenerative dementias: comparison with perfusion SPECT and with clinical evaluations lacking nuclear imaging. *J Nucl Med.* 2004;45:594–607.
30. Wierenga CE, Hays CC, Zlatar ZZ. Cerebral blood flow measured by arterial spin labeling MRI as a preclinical marker of Alzheimer's disease. *J Alzheimers Dis.* 2014;42(suppl 4):S411–S419.
31. Buckner RL. Memory and executive function in aging and AD: multiple factors that cause decline and reserve factors that compensate. *Neuron.* 2004;44:195–208.
32. Caroli A, Geroldi C, Nobili F, et al. Functional compensation in incipient Alzheimer's disease. *Neurobiol Aging.* 2010;31:387–397.
33. Besson FL, La Joie R, Doeuvre L, et al. Cognitive and brain profiles associated with current neuroimaging biomarkers of preclinical Alzheimer's disease. *J Neurosci.* 2015;35:10402–10411.
34. Rodell A, Aanerud J, Braendgaard H, Gjedde A. Washout allometric reference method (WARM) for parametric analysis of [^{11}C]PIB in human brains. *Front Aging Neurosci.* 2013;5(45):1–14.
35. Gjedde A, Aanerud J, Braendgaard H, Rodell AB. Blood-brain transfer of Pittsburgh compound B in humans. *Front Aging Neurosci.* 2013;5:70.